Linking Auxin with Photosynthetic Rate via Leaf Venation

Mcadam, Scott A. M.; Eléouët, Morgane P.; Best, Melanie; Brodribb, Timothy J.; Murphy, Madeline Carins; Cook, Sam D.; Dalmais, Marion; Dimitriou, Theodore; Gélinas-Marion, Ariane; Gill, Warwick M.; Hegarty, Matthew; Hofer, Julie M. I.; Maconochie, Mary; Mcadam, Erin L.; McGuiness, Peter; Nichols, David S.; Ross, John J.; Sussmilch, Frances C.; Urquhart, Shelley

Published in:
Plant Physiology

DOI:
10.1104/pp.17.00535

Publication date:
2017

Citation for published version (APA):
Mcadam, S. A. M., Eléouët, M. P., Best, M., Brodribb, T. J., Murphy, M. C., Cook, S. D., Dalmais, M., Dimitriou, T., Gélinas-Marion, A., Gill, W. M., Hegarty, M., Hofer, J. M. I., Maconochie, M., Mcadam, E. L., McGuiness, P., Nichols, D. S., Ross, J. J., Sussmilch, F. C., & Urquhart, S. (2017). Linking Auxin with Photosynthetic Rate via Leaf Venation. *Plant Physiology*, *175*(1), 351-360. https://doi.org/10.1104/pp.17.00535

Linking Auxin with Photosynthetic Rate via Leaf Venation[1][OPEN]

Scott A. M. McAdam,[a] Morgane P. Eléouët,[b] Melanie Best,[1] Timothy J. Brodribb,[a] Madeline Carins Murphy,[a] Sam D. Cook,[a] Marion Dalmais,[c] Theodore Dimitriou,[a] Ariane Gélinas-Marion,[a] Warwick M. Gill,[e] Matthew Hegarty,[b] Julie M. I. Hofer,[b] Mary Maconochie,[a] Erin L. McAdam,[a] Peter McGuiness,[a] David S. Nichols,[d] John J. Ross,[a] Frances C. Sussmilch,[a] and Shelley Urquhart[a]

[a]School of Biological Sciences, University of Tasmania, Hobart, TAS, 7001, Australia
[b]Institute of Biological, Environmental and Rural Sciences, Aberystwyth University, Aberystwyth SY23 3EE, United Kingdom
[c]Institue of Plant Sciences, Paris Saclay IPS2, CNRS, INRA, Université Paris-Sud, Université Evry, Université Paris-Saclay, Baitment 630, 91405 Orsay, France
[d]Central Science Laboratory, University of Tasmania, Hobart, TAS, 7001, Australia
[e]Tasmanian Institute of Agriculture and School of Land and Food, University of Tasmania, Hobart, TAS, 7001, Australia

ORCID IDs: 0000-0002-9625-6750 (S.A.M.M.); 0000-0002-1389-5654 (M.P.E.); 0000-0002-4964-6107 (T.J.B.); 0000-0003-4370-9485 (M.C.M.); 0000-0003-0950-6131 (S.D.C.); 0000-0002-1673-3095 (M.D.); 0000-0003-0446-6193 (A.G.-M.); 0000-0002-0158-7574 (G.M.I.H.); 0000-0003-2871-2774 (P.M.); 0000-0002-8066-3132 (D.S.N.); 0000-0003-3665-2062 (J.J.R.); 0000-0002-8659-1125 (F.C.S.); 0000-0002-8680-6720 (S.U.).

Land plants lose vast quantities of water to the atmosphere during photosynthetic gas exchange. In angiosperms, a complex network of veins irrigates the leaf, and it is widely held that the density and placement of these veins determines maximum leaf hydraulic capacity and thus maximum photosynthetic rate. This theory is largely based on interspecific comparisons and has never been tested using vein mutants to examine the specific impact of leaf vein morphology on plant water relations. Here we characterize mutants at the *Crispoid* (*Crd*) locus in pea (*Pisum sativum*), which have altered auxin homeostasis and activity in developing leaves, as well as reduced leaf vein density and aberrant placement of free-ending veinlets. This altered vein phenotype in *crd* mutant plants results in a significant reduction in leaf hydraulic conductance and leaf gas exchange. We find *Crispoid* to be a member of the *YUCCA* family of auxin biosynthetic genes. Our results link auxin biosynthesis with maximum photosynthetic rate through leaf venation and substantiate the theory that an increase in the density of leaf veins coupled with their efficient placement can drive increases in leaf photosynthetic capacity.

A central requirement for photosynthesis on land is the uptake of CO_2 from the atmosphere. To assimilate just one molecule of atmospheric CO_2, plants on average lose 150 molecules of water (Wong et al., 1979). To supply this high demand for water an internal transport system comprised of xylem conduits irrigates the leaf. Higher rates of photosynthesis (A) are linked to higher rates of transpiration, thus demanding greater efficiency in the transport and delivery of water to evaporating leaf tissue (Brodribb and Feild, 2000; Tyree and Zimmermann, 2002; Sack and Scoffoni, 2013). The xylem transports water efficiently through nonliving tubular cells in the leaf, yet the last part of the pathway involves a significantly slower transfer through living mesophyll cells to the stomata. The length of this final nonxylem transfer has a major influence on the efficiency of the entire water transport system (Brodribb et al., 2007). Current theory posits that as hydraulic supply is essential for A, a reduction in the mean path length for water flow through the mesophyll will increase leaf hydraulic conductance (K_{leaf}), which will increase stomatal conductance (g_s) and consequently theoretical maximum A (Sack and Frole, 2006; Brodribb et al., 2007, 2010; Scoffoni et al., 2011, 2016).

A core body of literature has identified a number of adaptations that reduce the terminal path length for water flow in the leaf and thus increase K_{leaf}. These adaptations range from increasing the density of the veins per unit area of leaf (Brodribb et al., 2007; Sack et al., 2013; Caringella et al., 2015), modifying leaf thickness and bundle sheath extensions (Sack et al., 2003; Zsögön et al., 2015) through to the formation of accessory transfusion tissue (Brodribb and Holbrook, 2005), and the formation and placement of free-ending veinlets (FEVs) within areoles (the small area of leaf mesophyll bound on all sides by veins; Scoffoni et al., 2011; Fiorin et al., 2016). Of these adaptations, vein density has been a major focus due to the high plasticity of this trait both within species (Carins Murphy et al., 2012; Scoffoni et al., 2015) and across vascular plant taxa (Boyce et al., 2009). Using this variation in vein density, strong correlations have been established

between the terminal path length for water flow through the mesophyll and maximum K_{leaf} (Sack and Frole, 2006; Brodribb et al., 2007, 2010; Sack et al., 2013; Scoffoni et al., 2016). These correlations are supported by single-gene vein density mutants in Arabidopsis (*Arabidopsis thaliana*) and *Solanum lycopersicum* spanning a spectrum of vein modifications that influence K_{leaf} (Caringella et al., 2015; Zsögön et al., 2015).

The importance of K_{leaf} lies in its positive correlation with A. Selection for greater A and productivity is believed to have been the primary driver behind the >10-fold increase in vein density that is observed in the fossil record over the past 400 million years, from the single-veined leaves of lycophytes to the highly complex, hierarchical networks of leaf veins in angiosperms (Brodribb et al., 2005; Boyce et al., 2009; Zhang et al., 2014). This increase in vein density is correlated with an equally substantial increase in maximum A across extant lineages that diverged during this major transition in leaf anatomy. Similar correlations between vein density, K_{leaf}, and A can be observed within angiosperms (Brodribb and Feild, 2010; Carins Murphy et al., 2012; Scoffoni et al., 2015, 2016).

However, this correlative evidence does not prove that changes in venation are responsible for changes in A, especially considering that stomatal and/or epidermal traits, which can also strongly influence maximum leaf gas exchange, are highly coordinated with vein density (Brodribb and Jordan, 2011; Carins Murphy et al., 2012, 2016). Here we use the powerful tool of physiological genetics to address the relationships between venation, water transport, and A. A number of mutants, particularly those related to auxin biosynthesis or signaling, have reduced vein densities, aberrant vein topologies, or defective vein formation (Tobeña-Santamaria et al., 2002; Scarpella and Meijer, 2004; Cheng et al., 2006, 2007; Verna et al., 2015). Indeed, the auxin canalization theory, based on observations of a self-organizing flux of auxin that initiates a vascular cambium, effectively predicts the formation and development of leaf vein networks (Sachs 1981; Lee et al., 2014; Rolland-Lagan and Prusinkiewicz, 2005). While the vein-patterning mutant resource has been invaluable for studying both auxin biosynthesis and the role of the auxin stream in leaf vascular formation, no study to date has examined whether these mutations affect vein networks independently of changes in stomatal density or anatomy, and if so, whether these vein defects influence K_{leaf}, maximum leaf gas exchange, and most importantly, A.

In this study, we characterize mutations at the *Crispoid* (*Crd*) locus of pea (*Pisum sativum*; Swiecicki, 1989; Berdnikov et al., 2000). We show that *Crd* corresponds to the *PsYUC1* gene, a member of the *YUCCA* gene family known to encode key auxin biosynthesis enzymes (Zhao et al., 2001; Mashiguchi et al., 2011). We comprehensively describe aberrations in the vein morphology, topology, maximum leaf gas exchange, and K_{leaf} in the *crd-4* mutant. We use this mutant to test the hypothesis that maximum A is determined by the distance water must travel through the mesophyll. We show that maximum A is regulated by auxin through leaf venation.

RESULTS

crd Mutants Carry Lesions in the Pea Homolog of AtYUC1/AtYUC4/PhFLOOZY

Homozygous recessive *crd* mutants are easily distinguished from wild-type (Swiecicki, 1989; Berdnikov et al., 2000) plants due to a noticeable reduction in vein density (Fig. 1, A and B; Supplemental Table S1). Two mutants with similar defective venation phenotypes were identified and shown to be additional alleles of the *Crd* locus by complementation testing (Supplemental Fig. S1). The recessive mutant alleles were named *crd-1* (Swiecicki, 1989), *crd-2* (Berdnikov et al., 2000), *crd-3* (FN 1522/1), and *crd-4* (UTILLdb L905). To identify the gene affected in the *crd* mutants, we used a next-generation RNA sequencing approach, focusing on the identification of any transcripts missing from the *crd-3* allele, as most lesions characterized so far from the JI 2822-derived fast-neutron mutant population have been large, gene-sized deletions (Domoney et al., 2013). We assembled a reference transcriptome from the corresponding wild-type line (WT-3) comprising 79,693 contigs (N50 = 1,191 bp), and used this reference transcriptome to map reads from triplicate *crd-3* samples. We identified two contigs that showed significant differences in expression between the *crd-3* and WT-3 genotypes (false-discovery rate [FDR] corrected P value < 0.05). Only one contig, 435 bp in length,

[1] The TILLING platform was supported by the ERC Advanced Grant SEXYPARTH (M.D.). This work was supported by the Australian Research Council (grant nos. DE140100946 [S.A.M.M.], DP140100666 [T.J.B.], and DP130103357 [J.J.R.]).

[2] Address correspondence to smcadam@utas.edu.au.

The author responsible for distribution of materials integral to the findings presented in this article in accordance with the policy described in the Instructions for Authors (www.plantphysiol.org) is: Scott A.M. McAdam (smcadam@utas.edu.au).

S.A.M.M. developed the research plans for and supervised measurements of anatomy, gas exchange, and hydraulics and wrote the manuscript with contributions from J.M.I.H. and M.P.E. who designed the research plans for molecular and phenotypic characterization of mutant alleles; A.G.-M. performed auxin quantifications and auxin activity analyses and wrote the relevant sections; S.D.C. prepared phylogenetic analyses and wrote the relevant sections; F.C.S. molecularly characterized a mutant allele and wrote the relevant sections; E.L.M. acquired lines for auxin activity analyses; M.B., T.D., M.M., S.U., and M.C.M. collected anatomical and physiological data; P.M. designed specialized software for anatomical analyses; M.D. developed a mutant allele; D.S.N. assisted in the quantification of auxin; W.M.G. undertook resin imbedding; M.H. supervised and assisted in the characaterization of a mutant allele; T.J.B. assisted in experimental design; and J.J.R first observed the *pss* allele and complemented the writing.

[OPEN] Articles can be viewed without a subscription.
www.plantphysiol.org/cgi/doi/10.1104/pp.17.00535

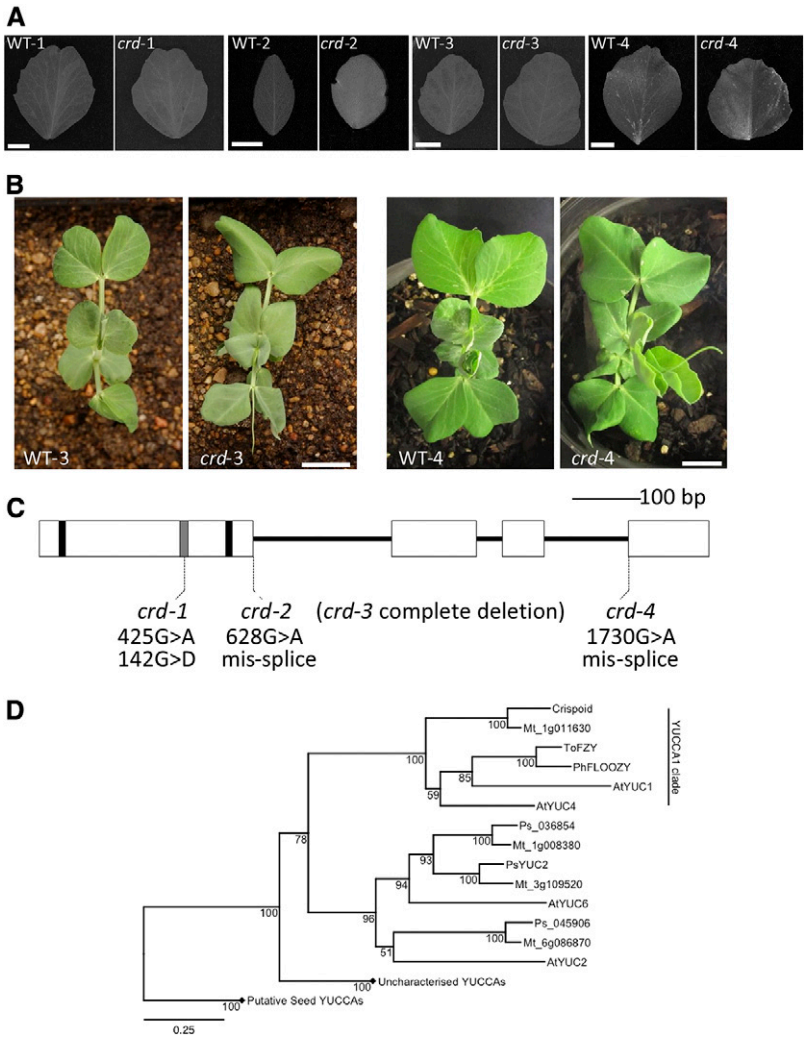

Figure 1. A, Representative leaflets from node 6 taken from each *crd* mutant allele and respective wild type. A 1-cm scale marker for each pair is shown in the wild-type image of each pairing. B, Aerial view of seedlings of WT-3 and *crd-3* (left) and WT-4 and *crd-4* (right) showing node 4 leaves uppermost in each panel. A 2-cm scale marker for each pair of images is shown on the mutant image of each pairing. Similar images or comprehensive phenotypic details of *crd-1* and *crd-2* seedlings are provided by Swiecicki (1989) and Berdnikov et al. (2000), respectively. C, Diagram of *Crd* gene showing regions encoding conserved motifs and the positions of *crd* mutations. Exons are shown as boxes, nucleotides encoding FAD- and NADPH-binding motifs are shown as black bars, ATG-containing motif 1 is shown as a gray bar. D, Phylogenetic analysis of YUCCA protein sequences from *M. truncatula* (Mt), pea (Ps), and Arabidopsis (At), as well as ToFZY (*Solanum lycopersicum*) and PhFLOOZY (*Petunia hybrida*). Bootstrap values (from 1,000 iterations) for this BIONJ tree are displayed adjacent to nodes, and the scale bar indicates genetic distance (0.25 changes/amino acid). Diamonds indicate collapsed clades belonging to the putative but uncharacterized seed YUCCA clades. Accession numbers for all genes are given in Supplemental Table S2.

was expressed in WT-3 samples but showed complete absence of expression in *crd-3* mutant samples, consistent with a fast neutron-generated deletion. This contig corresponded to the entire last exon and portion of the 3′ UTR of *PsYUC1*, a previously identified pea homolog of *AtYUC1*/*AtYUC4*/*PhFLOOZY*, encoding a 411-amino acid flavin-containing mono-oxygenase (FMO) protein (Tivendale et al., 2010).

To test whether *PsYUC1* corresponds to the *Crd* locus, the four known *crd* mutant alleles were characterized further. We identified a 425G > A SNP in the *crd-1* allele (Fig. 1C), which would result in a 142G > D amino acid substitution within the ATG-containing motif 1 conserved between YUCCA proteins (Liu et al., 2012). A single 628G > A SNP was identified in the coding sequence of the *crd-2* allele, which is predicted to cause an intron 1 splicing defect (Fig. 1C). Accordingly, PCR analysis of *crd-2* cDNA showed several transcripts of different sizes (Supplemental Fig. S2). Sequencing confirmed that the largest of these transcripts contained the unspliced intron 1, which would encode a protein product with a frameshift at position 210 and premature termination after 244 amino acids (Supplemental Fig. S3). A smaller misspliced *crd-2* transcript was found to contain 4 bp of intron 1, which would also result in a frameshift at position 210 and premature termination of the protein product after 262 amino acids. No portion of the *PsYUC1* gene could be amplified from *crd-3* genomic DNA template using PCR primer pairs spanning the full length of the gene, suggesting that *crd-3* is a null allele corresponding to complete deletion of *PsYUC1* (Supplemental Fig. S4). The *crd-4* allele was characterized as a 1730G > A SNP, which would shift the intron 3 splice acceptor site 1 bp downstream relative to WT-4. This would cause a frameshift at position 334 of the protein product, with 27 nonsense amino acids preceding premature termination of the protein.

Crd and *PsYUC1* cosegregated in an F_3 population of 96 individuals, which is consistent with these representing the same locus. Furthermore, genetic mapping located *PsYUC1* on pea LG II, at a position consistent with the *Crd* locus. On the basis of the strong evidence

provided by these RNA-seq data, cosegregation analysis and the significant lesions characterized in four independent alleles, we concluded that the *Crd* locus corresponds to the *PsYUC1* gene. Phylogenetic analysis revealed that of the 12 *FMO* genes most closely related to *AtYUC1/AtYUC4/PhFLOOZY* identified in the pea gene atlas (Alves-Carvalho et al., 2015), *Crd* is the only gene that groups with members of the *AtYUC1/AtYUC4/PhFLOOZY/SlFZY* clade (Fig. 1D), indicating that *Crd* is the pea ortholog. This conclusion is further supported by the finding that there is also only a single *Medicago truncatula* gene, Medtr1g011630, that groups within this clade present in the genome of *M. truncatula* (Fig. 1D). *M. truncatula* is a sequenced legume closely related to pea, and their genomes are collinear in this region (Tayeh et al., 2015). Reciprocal BLASTn searches of the *M. truncatula* genome (v4) and pea transcriptome databases showed that *Crd* is most similar to Med1g011630; they likely represent an orthologous pair.

Altered Vein Topology in *crd* Mutants

A common feature of all *crd* mutant alleles is a reduction in vein density at both a macroscopic and microscopic level (Figs. 1, A and B and 2, A and B; Supplemental Table S1). Major vein density is reduced in the mutant alleles, with a significant reduction in the density of either or both secondary and tertiary orders of veins in mutants compared to wild-type leaves (Fig. 1A; Supplemental Table S1). A more comprehensive microscopic examination of *crd-4* mutant leaves revealed a 20% reduction in minor vein density compared to WT-4 leaves (Fig. 2C). This reduction is not associated with changes in stomatal density or stomatal size, with both of these traits being the same as in WT-4 plants (Fig. 2, D and E). The placement and development of FEVs in areoles was also severely altered in the *crd-4* mutant (Fig. 3). In WT-4 plants, the mean distance from the stomata to the nearest vein showed little variability across the spectrum of areole sizes. In contrast, and consistent with observations of lower vein density, *crd-4* mutants had a significantly greater mean distance from the stomata to the nearest vein compared to WT-4 across areole sizes (*t* test, $P < 0.001$), as well as a significantly greater variance in the mean distance from stomata to the nearest vein (F-test, $P < 0.001$; Fig. 3). The development of FEVs was substantially reduced in *crd-4* mutant plants compared to WT-4 plants (Fig. 3, B and C), which in addition to a lower vein density contributed to the greater mean distance from stomata to the nearest vein. In WT-4 plants, only 60% of the smallest size class of areoles lacked FEVs, with all areoles larger than 0.15 mm^2 having these structures (Fig. 3B). In *crd-4* plants, all areoles <0.15 mm^2 lacked FEVs, and only areoles >0.5 mm^2 consistently developed FEVs in this mutant (Fig. 3C).

Leaf Hydraulic Capacity and Gas Exchange in *crd* Mutants

Maximum K_{leaf} was reduced in *crd-4* mutant plants, being 30% lower than in WT-4 plants (Fig. 4). Leaf gas exchange was also significantly reduced in the *crd-4* mutant plants compared to WT-4 plants at both high and low vapor pressure deficit (VPD; Fig. 4). Leaf gas exchange parameters including A and g_s in WT-4 plants were double that of *crd-4* plants at low VPD and significantly higher at high VPD (Fig. 4). Photosynthetic apparatus was not compromised by the *crd-4* mutation, with both WT-4 and *crd-4* plants having similar A-internal CO_2 concentration (C_i) relationships (Supplemental Fig. S5). The lower maximum A observed in *crd-4* mutant plants is likely to have contributed to a reduction in shoot

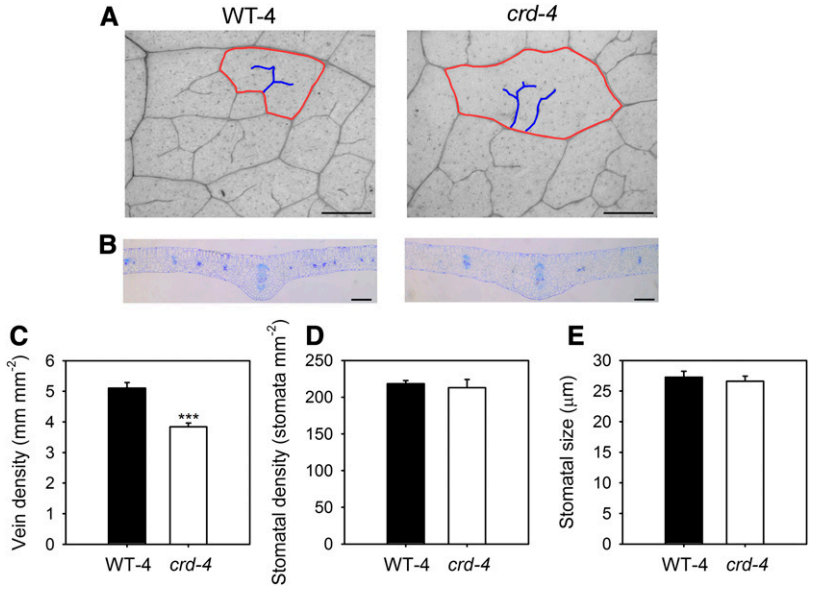

Figure 2. A, A representative longitudinal image of leaf venation in WT-4 and *crd-4* leaves (scale bar = 200 μm, red lines outline an areole, blue lines highlight FEVs within the areole). B, A representative cross-sectional image of WT-4 and *crd-4* mutant leaves through the midrib (scale bar = 200 μm). C, Mean vein density (n = 7 leaves, ±SE), D, stomatal density (n = 7 leaves, ±SE), and E, stomatal size (n = 50 stomata, ±SE) in WT-4 and *crd-4* mutant plants. Asterisks denote significant difference in means ($P < 0.001$).

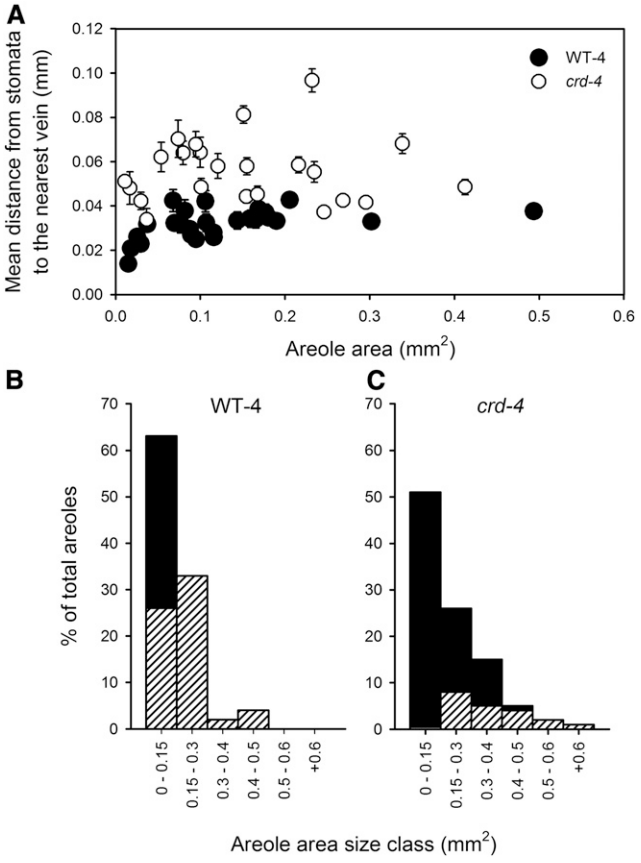

Figure 3. A, The relationship between the mean distance from stomata to the nearest vein (including FEV) in an areole (±SE) and areole area for WT-4 (white circles) and *crd-4* mutant (black circles) plants. FEV occurrence across size classes of areoles in WT-4 (B) and *crd-4* (C) mutant plants; bars represent the percentage of areoles that fall within each size class, with hatching depicting the areoles in that size class that had FEVs.

biomass observed in these plants compared to WT-4 plants (Supplemental Fig. S6). Other factors may contribute to reduced growth in the *crd* mutants, which, in addition to altered vein anatomy, have an occasional reduction or modification in tendril number as well as, rarely, leaflet/pinna number (Supplemental Figs. S7 and S8).

Mutation in *Crd* Reduces Auxin Activity and Levels in Expanding Leaves

FMO enzymes are believed to catalyze the conversion of indole-3-pyruvic acid to auxin (indole-3-acetic acid [IAA]; Mashiguchi et al., 2011). To visualize potential differences in auxin activity in the developing leaves of *crd-4* and WT-4 plants, we utilized a *DR5::GUS* reporter construct, for which *GUS* expression is driven by the promoter of a highly active synthetic auxin response element (DeMason and Polowick, 2009). A substantial reduction in auxin activity was noted in the veins of developing leaves of *crd-4 DR::GUS* plants compared with those of WT-4 *DR5::GUS* plants, by minimal *GUS* staining (Fig. 5A). In contrast to WT-4 leaves, no *GUS* staining was observed in young leaves (<4 mm in length) of *crd-4 DR5::GUS* plants, indicating reduced auxin activity (Supplemental Fig. S9). We further investigated this difference in auxin activity in developing leaves by quantifying the levels of both free IAA and the auxin conjugate, IAA-Asp (IAAsp), in apical tissue containing developing leaves and meristematic tissue. Free IAA and IAAsp levels were reduced by approximately 50% and 80%, respectively, in the apical tissue of *crd-4* plants compared to WT-4 plants (Fig. 5, B and C). In contrast, a reduction in free IAA levels was not observed in whole shoots (Supplemental Fig. S10).

DISCUSSION

Auxin via Vein Anatomy Drives Maximum Leaf Gas Exchange

Current theory indicates that the terminal path length for water flow through the mesophyll should govern maximum K_{leaf} (Buckley et al., 2015), g_s, and thus maximum A (Brodribb et al., 2010). However, both parts of this proposition are supported largely by correlative evidence, derived from natural variation within and between species (Sack and Frole, 2006; Brodribb et al., 2007;

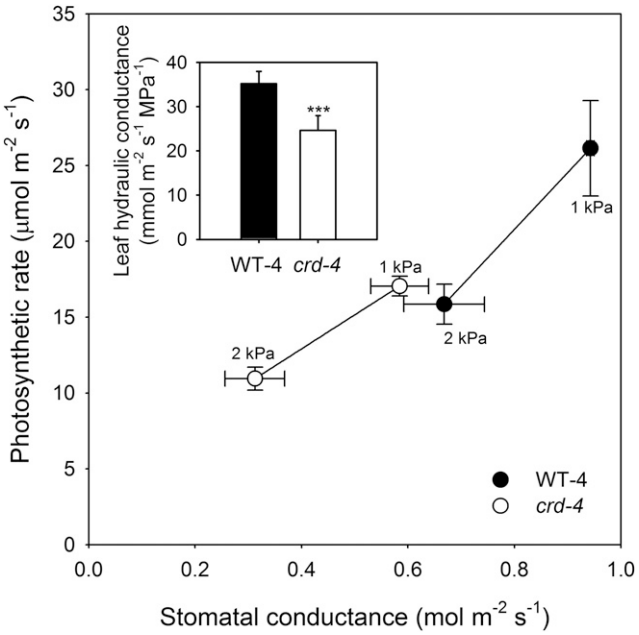

Figure 4. Mean photosynthetic rate and stomatal conductance ($n = 3$; ±SE) measured in leaves of whole plants exposed to a VPD of 1 or 2 kPa in WT-4 (black circles) and *crd-4* mutants (white circles). Insert depicts mean maximum leaf hydraulic conductance ($n = 6$; ±SE) in WT-4 and *crd-4* mutant plants. Asterisks denote a significant difference in means ($P < 0.001$).

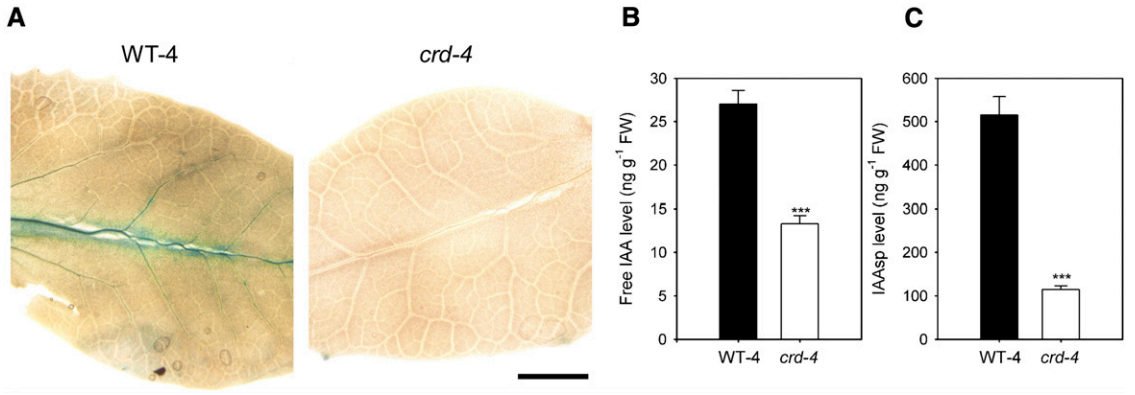

Figure 5. A, GUS expression in expanding pinnae of representative F2 segregant plants (<8 mm in length) taken from WT-4, *DR5::GUS,* and *crd-4, DR5::GUS* plants (scale bar = 2 mm). B, Mean levels of IAA and IAAsp (C) from apical tissue of WT-4 and *crd-4* mutant plants ($n = 4$, ±SE). Asterisks denote a significant difference in means ($P < 0.001$).

Brodribb and Feild, 2010; Scoffoni et al., 2015, 2016). Recently, the influence of the distance through the mesophyll for water flow on K_{leaf} was demonstrated experimentally using a genetic approach (Caringella et al., 2015), and here we present genetic evidence that auxin, through leaf venation, acts as a regulator of both maximum leaf hydraulic supply and maximum A, and likely whole plant productivity. Our physiological analyses of the auxin-biosynthetic *crd* mutants indicate that altered vein density and topology results in an increase in the hydraulic path length for water flow through the mesophyll, reduced maximum K_{leaf}, and as a consequence maximum A. Our data support the conclusions derived from correlations that have highlighted the importance of an efficient internal leaf water transport system for maximizing both g_s and A (Sack and Frole, 2006; Brodribb et al., 2007; Carins Murphy et al., 2012).

The effects of auxin deficiency on water transport, and consequently A, observed in the *crd-4* mutant occurred independently of any changes in stomatal anatomy, photosynthetic apparatus, or intrinsic photosynthetic capacity. This breaking of coordination between vein and stomatal development is surprising, given that angiosperms are extremely efficient at coordinating hydraulic supply (the formation of veins) with demand (the density of stomata; Brodribb and Jordan, 2011; Carins Murphy et al., 2016). The absence of a distinctive stomatal phenotype in the *crd-4* mutant plants is at odds with the suggestion that auxin transport influences stomatal development (Le et al., 2014). Interestingly, there have been no reports of aberrant vein development in the collection of stomatal patterning mutants (Berger and Altmann, 2000; Kanaoka et al., 2008), which suggests independent pools of auxin must be involved in the developmental regulation of these two morphological features. The endogenous signal that may be responsible for coordinating vein and stomatal density in a developing leaf thus remains unknown.

The Formation of FEVs

In addition to providing experimental evidence for the link between maximum K_{leaf} and A, our observations of the *crd-4* mutant revealed substantial rearrangements in the topology of the leaf vein network. We found that, unlike in WT-4 plants, both major and minor vein density were reduced in mutant plants and, in contrast to a wide diversity of angiosperms species (Fiorin et al., 2016), the development of FEVs in both large and small areoles in *crd-4* plants was affected, as evidenced by a greater distance from stomata to the nearest vein in all size classes of areoles. Recent work has suggested that a strong selective pressure is placed on plants to develop leaves with a uniform distance from the nearest vein to the stomata (Fiorin et al., 2016). The correct positioning of FEVs minimizes the mean distance from the minor veins to the nearest stomata. The mechanism regulating this key anatomical feature of reticulate veined angiosperm leaves is unknown; however, auxin clearly plays a major role.

Auxin Biosynthesis as a Central Regulator in the Formation of Veins

Auxin biosynthesis in plants occurs through a two-step pathway from the amino acid Trp to IAA via the intermediate indole-3-pyruvic acid (Zhao, 2012). These two steps are sequentially catalyzed by Trp aminotransferases and FMOs from the YUCCA family (Tao et al., 2008; Mashiguchi et al., 2011). We show here that *Crd* is the only transcript recovered from pea database searches that is embedded within the clade of FMO auxin biosynthetic genes, including *YUCCA1* and *YUCCA4* from Arabidopsis and *FLOOZY* from Petunia (*Petunia hybrida*; Fig. 1D). Consistent with this, we found reduced free IAA levels in *crd-4* apical tissue when compared with WT-4 plants (Fig. 5B). This finding demonstrates the importance of local auxin synthesis in the early stages of leaf and vascular

development. In addition to reduced IAA levels, our observation of substantially lower levels of IAAsp in the apical tissue of *crd-4*, compared to WT-4 plants, is indicative of impaired IAA biosynthesis in the apical bud. Interestingly, we observed no difference in free IAA levels in whole shoot tissue of seedlings of the *crd-4* mutant plants compared to WT-4 plants (Supplemental Fig. S10), suggesting the reduction in auxin levels in these mutants is localized to the developing leaves. Our *DR5::GUS* reporter observations further support this, indicating that a reduction in IAA levels may be localized to the developing vascular tissue in expanding leaves of mutant plants (Fig. 5A). In wild-type plants, high auxin activity in vascular tissue of developing leaves has been reported previously in pea (Demason et al., 2013) as well as Arabidopsis (Mattsson et al., 2003); in *crd-4* leaves we found no *GUS* staining apparent in the developing veins (Fig. 5A). Similar reductions in *GUS* staining have been observed in the veins of multiple *yuc* mutants in Arabidopsis lines carrying a *DR5::GUS* reporter (Cheng et al., 2006). Furthermore, systemic reductions in auxin activity were also noted in very young developing leaves of *crd-4* mutant plants (Supplemental Fig. S9).

The development of the leaf vascular network can be explained by the auxin canalization theory, which describes a self-forming auxin transport stream initiating the formation of a vascular cambium (Sachs 1981). The profound and highly dysfunctional vein phenotypes of mutants in PIN-FORMED proteins strongly implicate auxin efflux as a major regulator of this auxin transport stream and thus the formation of leaf veins (Mattsson et al., 1999). As a result, modifications to the auxin transport stream by auxin efflux dominates models seeking to simulate vein patterning (Bennett et al., 2014; Feugier et al., 2005; Lee et al., 2014; Mitchison, 1980; Rolland-Lagan and Prusinkiewicz, 2005). Our results, however, add to previous evidence suggesting that, in addition to auxin efflux rates, the biosynthesis of this hormone also plays an important role in establishing a normal leaf vascular network (Tobeña-Santamaria et al., 2002; Cheng et al., 2006, 2007). Indeed, Cheng et al. (2007) found that auxin deficiency on a background of reduced auxin efflux had an additive effect on compromised leaf vascular development. Whether current models for leaf venation patterning, based primarily on auxin efflux dynamics, can mimic venation patterns observed in auxin biosynthetic mutants or require substantial modification will be an interesting avenue for future research.

Auxin as a Driver of Maximum Photosynthetic Rate

The importance of *Crd*, an FMO, in normal vein formation and thus maximum *A* suggests that this clade of auxin biosynthetic genes has been central to the formation of complex, high-density vein networks in the leaves of derived angiosperms, a prerequisite for the high productivity of these species (Scoffoni et al., 2016). Phylogenetic analysis of closely related FMOs suggests that duplication and functional specialization in this family occurred prior to and during the diversification of angiosperms, allowing for the evolution of a clade of genes that play key roles in the development and topology of veins. This clade includes *Crd*, *PhFLOOZY*, *AtYUCCA1*, and *AtYUCCA4*, which all result in compromised leaf vascular development when mutated (Tobeña-Santamaria et al., 2002; Cheng et al., 2006, 2007). Given the importance of auxin in the development of efficient reticulate venation patterns in angiosperms, it is an intriguing possibility that this hormone may have played an instrumental role in the Cretaceous radiation and ecological rise of the angiosperms. Indeed, as the hydraulic pathway through the leaf accounts for the greatest limitation to maximum realized leaf gas exchange, whether enhancing auxin levels in a developing leaf will improve maximum productivity remains to be tested. However, our new mechanistic understanding of auxin as a key developmental determinant of maximum leaf gas exchange provides exciting potential for future increases in plant productivity.

MATERIALS AND METHODS

Plant Material

Previously described *crd* mutants include the first described allele (*crd-1*; JI 2460) selected after N-ethyl-N-nitrosourea mutagenesis of the line Paloma (WT-1; Swiecicki, 1989) and the *crispoid-whip* allele (*crd-2*; JI 3160), found after ethyl methane sulfonate mutagenesis of the line SG (WT-2; Berdnikov et al., 2000). These mutants were obtained from the John Innes *Pisum* Germplasm collection. In this paper, two novel *crd* mutant alleles were identified. The *crd-3* mutant was identified as line FN 1522/1 in a fast neutron mutagenesis population of the JI 2822 line (WT-3; Domoney et al., 2013). The *crd-4* mutant was observed incidentally in line 905, derived from an ethyl methane sulfonate mutagenesis population of the Caméor line in the UTILLdb program (Dalmais et al., 2008). Initially this mutant was named *pipes in short supply* (*pss*). Allelism was confirmed by noncomplementation of the *crd* phenotype in F1 progeny from the crosses of FN1522/1 × *crd1*, FN1522/1 × *crd2*, and *pss* × *crd1* (Supplemental Fig. S1). At least six generations of backcross selection were undertaken to provide near-isogenic wild-type (WT-4) and *crd-4* lines for morphological and physiological experiments. Three generations of backcross selection were undertaken to provide *crd-3* lines for RNA sequencing.

crd-1, *crd-2*, *crd-3*, and respective wild-type plants (as well as plants from allelism tests between these lines) were sown in a glasshouse in Aberystwyth, UK, under natural light between June and September (5.2–9.5/18.2–22.4°C day/night temperatures) in peat-free Jiffy pellets 7C, 45 × 40 mm (Jiffy products S.L. (pvt) Ltd) and after 2 weeks transferred into 12-cm-long and 12-cm-diameter pots with John Innes potting mix number 3 (http://www.johninnes.info/about.htm) supplemented with 30% chick grit. Jiffy pellets and pots were placed on a carpet that was watered every day, allowing the plants to absorb water through the carpet. WT-4 and *crd-4* plants (and plants for the allelism test with this line, as well as *DR5::GUS* reporter lines) were grown under the controlled glasshouse conditions in Hobart, Australia, described by McAdam et al. (2016). All morphological and physiological observations were made on fully expanded node 4 leaves, unless specified otherwise.

RNA-Sequencing and Sequence Data Analysis to Identify the crd-3 Mutation

Total RNA from 20-d-old *crd-3* and WT-3 shoot tips (three replicates each) was extracted using the RNeasy Plant Mini Kit (Qiagen), and RNA concentration was determined using a Qubit fluorescence spectrophotometer (Thermo Fischer). Each amplified library for sequencing was prepared from 2 μg of total RNA (Illumina TruSeq RNA v2 Sample Preparation Kit) and uniquely indexed to enable multiplex sequencing. Libraries were analyzed by gel electrophoresis

and quantified using Qubit and then adjusted to 10 nM in 0.1 M Tris-HCl/0.01% (v/v) Tween 20 buffer and pooled equally prior to denaturation/dilution in a final loading concentration of 8 pM. Uniquely indexed, amplified libraries prepared for RNA-seq were typically 300 bp in size. These were multiplexed and sequenced in 2 × 126-bp format in a single lane of a HiSeq v4 high-output flowcell on an Illumina HiSeq2500 platform. Data in FASTQ format were analyzed using the Genomics Workbench v6.5 software package (CLC Bio). RNA-seq data obtained ranged from 68.3 to 79.5 million reads per sample for *crd-3* (average 73 million) and from 73 to 90 million reads for WT-3 (average 80.4 million). Following trimming to remove low-quality sequence and reads <50 bp, these were reduced to an average of 71.4 million reads for *crd-3* and 78.9 million reads for WT-3, with an average read length of 113 bp for all samples. Overlapping WT-3 read-pairs were merged (approximately 54% of each wild-type dataset), and these data were used along with unmerged WT-3 read-pairs (21.85 Gbp in total) for de novo assembly of a reference transcriptome using the *de Bruijn* graph method with a k-mer value of 25. Maximum bubble size for conflict resolution within the graph was set at 50. Repeat regions within the graph were resolved using scaffolding based on paired-end sequences. Following initial contig assembly, reads were mapped back to contigs, requiring 50% identity and 80% similarity across the read. Ambiguous reads mapping to more than one contig were discarded. Insertion and deletion penalties were set at 3 and mismatch penalty at 2. Contigs from the initial assembly were removed if no reads mapped. Reads from all six individual samples were subsequently mapped to these reference contigs and used to calculate the number of reads mapped per kb of exon, per million mapped reads (RPKM; Mortazavi et al., 2008). On average, 85% of reads from each sample could be mapped to reference contigs and used to generate RPKM expression values. RPKM values were analyzed as a two-group experiment, *crd-3* versus WT-3, to identify significantly different expression values between the two groups, with *P* values adjusted using a FDR (Benjamini and Hochberg, 1995). One significantly different (FDR-corrected *P* value < 0.05) contig sequence, showing complete absence of expression in *crd-3* mutants, was used to query NCBI nucleotide and protein databases, using BLASTn and BLASTx, respectively, to identify the corresponding gene.

Sanger Sequencing for Mutant Characterization

For cDNA template preparation, total RNA was first extracted as for RNA sequencing and treated with DNase (Ambion; WT-1 to -3, *crd-1* to -3), or with the SV total RNA isolation system (Promega) including a DNase step (WT-4, *crd-4*), and quality-checked by gel electrophoresis. RNA was reverse-transcribed using oligo(dT) primers and the Superscript III First-Strand Synthesis System (Invitrogen) in a total volume of 50 μL containing 0.4 μg RNA (WT-1 and *crd-1*) or 0.2 μg RNA (WT-2 and *crd-2*; WT-3 and *crd-3*), or using the Tetro cDNA synthesis kit (Bioline) in 20 μL containing 1 μg RNA (WT-4 and *crd-4*). Genomic DNA template was extracted from leaves following the DNeasy Plant Mini Kit protocol (Qiagen; WT-1 to -3, *crd-1* to -3) or using a CTAB-based method (WT-4, *crd-4*; Allen et al., 2006). All primers are listed in Supplemental Table S3. Sanger sequencing of purified PCR products was performed at Aberystwyth University or by Macrogen Inc. (Korea).

Genetic Analysis

Plants grown in the glasshouse were scored for *crd* or wild-type phenotype. A WT-1 × *crd-1* cross yielded 96 F_3 progeny segregating 74:22 (3:1, $\chi^2 = 0.2$, $P > 0.6$, n.s.). To test for cosegregation of the *crd* phenotype and the *crd-1* mutation, phenotype and genotype scores of the F_3 progeny were compared. Genomic DNA prepared from each plant was genotyped using a cleaved-amplified polymorphic sequence marker for the *Crd* locus, amplified by PCR using primers 5F and 7R in Supplemental Table S1 and digested with *Dde*I. Digestion products were distinguished after gel electrophoresis (WT-1: 385 bp, 147 bp and 110 bp; *crd-1*: 385 bp and 257 bp). All plants homozygous for the *crd-1* allele had the *crd* phenotype, and no heterozygous plant or any plants homozygous for the WT-1 allele had the *crd* phenotype (χ^2= 93.2, $P = 6 \times 10^{-21}$). The same cleaved-amplified polymorphic sequence marker was used to place the *Crd* locus on the genetic map of the JI 281 × JI 399 recombinant inbred population (Laucou et al., 1998) at position 130 cM on LG II, between markers *cDNA39* and *SNP190*.

Phylogenetic Analysis

The phylogenetic relationships between *YUCCA*-related genes in Arabidopsis (*Arabidopsis thaliana*), *Medicago truncatula*, and pea (*Pisum sativum*) were assessed in conjunction with selected characterized genes from other species using amino acid sequences obtained from GenBank (www.ncbi.nlm.nih.gov) and the pea gene atlas (Alves-Carvalho et al., 2015; Supplemental Table S2). Sequences were aligned using the Clustal Omega algorithm (Sievers et al., 2011), and phylogenies were reconstructed using an LG substitution model (Le and Gascuel, 2008) based on a BIONJ tree using the statistical analysis software R. The packages APE (Paradis et al., 2004) and phangorn (Schliep, 2011) were used for sequence management and modeling, and ggtree (Yu et al., 2017) was used for tree visualization.

Leaf Anatomy

Leaves of *crd-1*, *crd-2*, and *crd-3* mutant lines and respective wild types were prepared for vein density measurements by incubating overnight in a solution of 3:1 ethanol:acetic acid (v/v) at room temperature. Leaves were then incubated for 1 h in a solution of 70% ethanol in water (v/v) and later transferred to 50% ethanol in water (v/v) until scanned at 600 to 1200 DPI (HP Scanjet 8200).

Paradermal sections of WT-4 and *crd-4* leaves were cleared in household bleach (50 g/L sodium hypochlorite and 13 g/L sodium hydroxide) and stained in 1% toluidine blue. Five fields of view (FOV) at 4× magnification (for vein density measurements, FOV: 3.47 mm^2), five FOV at 20× magnification (for stomatal density measurements), sufficient images at 40× magnification to capture 50 stomata (for measuring stomatal size), and images at 20× magnification focusing on the abaxial stomatal surface and covering the entire areole (for calculating mean stomatal distance to the nearest vein) were taken using a Nikon Digital Sight DS-L1 camera mounted on a Leica DM 1000 microscope. Vein density and stomatal density were measured using ImageJ, as the total length of leaf vascular tissue and total number of stomata per mm^2 of leaf area. Stomatal size was determined by measuring the longest distance parallel to the stomatal pore from the edges of the guard cells using ImageJ. The mean distance from stomata to the nearest vein for 24 areoles, randomly selected to span the full-size spectrum of areoles across the leaf, was determined by making a composite image of each areole using the 20× objective FOVs, which were then assembled together in Adobe Photoshop. This composite image of each areole was analyzed using specifically designed software that calculated the mean distance to the nearest vein for each stomata in the areole once veins and stomata were manually marked. Leaf cross-sections were made from leaf segments spanning the midrib that were fixed in 2.5% buffered glutaraldehyde under vacuum then dehydrated in acetone and embedded in Spurr's resin. Semithick sections (5–7 μm) were stained with toluidine blue O.

Leaf Gas Exchange and K_{leaf}

One leaf from three individuals of both WT-4 and *crd-4* were used to determine the response of leaf gas exchange to variation in VPD. A portable infrared gas analyzer (Li-6400; Li-Cor Biosciences) was used to measure leaf gas exchange between 1130 and 1300 h when gas exchange was expected to be maximal. Conditions within the leaf cuvette were maintained as close to external conditions as possible (temperature at 22°C and light intensity at 1,000 μmol m^{-2} s^{-1}, VPD was regulated relative to external conditions by controlling intake air flow through a desiccant column). On the first day of measurement, VPD in the glasshouse was held at 1 kPa from dawn by a dehumidifier with integrated humidity sensors (ADH-1000, Airrex Portable dehumidifier, Hephzibah Co. Ltd.); on the second day of measurement, VPD in the glasshouse was held at 2 kPa. On each day, midday leaf water potential was measured in all plants using a pressure chamber. K_{leaf} was measured in three leaves of WT-4 and *crd-4* plants using the evaporative flux method and flowmeter according to Carins Murphy et al. (2012).

Shoot Biomass and Growth

Whole shoots of WT-4 and *crd-4* plants (n = 3), grown under the same glasshouse conditions, were harvested 28 d after sowing and dried at 70°C for at least 62 h before being weighed (± 0.0001 g). Plant height in WT-1, *crd-1*, WT-3, and *crd-3* plants (n = 13–14), grown under the same glasshouse conditions, was measured every 10 d (from 20 d after sowing) until plants had dried at 60 d after sowing.

Quantification of Free IAA and IAAsp Levels

Growing apical tissue, including all tissue immediately proximal to the uppermost fully expanded leaf of WT-4 and *crd-4* plants, was harvested. Tissue was weighed (± 0.0001 g; with approximately 25 mg harvested per replicate for both genotypes) and placed in 1 mL of sodium phosphate buffer (50 nM, pH7).

Samples were homogenized with a bead mill for 2 min. To quantify the endogenous compounds, stable isotope-labeled internal standards were added; these were [$^{13}C_6$]-IAA (Cambridge Isotope Laboratories) and [^{15}N, $^{2}H_5$]-IAAsp (OlChemim). Compounds were extracted according to Novák et al. (2012). In addition, free auxin was quantified in two-week-old whole seedlings of WT-4 and *crd-4*, which were weighed and harvested into 3 mL of 80% methanol in water (v/v) containing 250 mg/L butylated hydroxytoluene. All samples were analyzed by ultra-performance liquid chromatography tandem mass spectrometry as described by Cook et al. (2016).

DR5::GUS Staining for Auxin Activity

Transgenic *DR5::GUS* lines carrying the WT-4 and *crd-4* alleles were constructed by crossing the RTP9 line (DeMason and Polowick, 2009) with *crd-4* mutant pollen. The segregating F2 generation consisting of 42 *Crd* GUS+: 15 *crd* GUS+: 14 *Crd* GUS-: 7 *crd* GUS- (9:3:3:1, $\chi^2 = 1.0$, $P = 0.8$, n.s.) was genotyped by PCR for *DR5::GUS* using the primers and conditions described by DeMason and Polowick (2009), and distinctive leaf morphology phenotypes were used to identify *crd-4* plants. Young developing leaflets <8 mm in length (one per individual, harvested from eight randomly selected individuals per genotype) were removed from within stipules enclosing the apical meristem and immediately immersed in GUS staining buffer containing 2 mM 5-bromo- 4-chloro-3-indolyl b-D-glucuronide, 100 mM sodium phosphate (pH 7.5), 0.5 mM potassium ferricyanide, 0.5 mM potassium ferrocyanide, 10 mM EDTA, and 0.1% (v/v) Triton X-100. Samples were vacuum-infiltrated on ice at 200 mbar for 45 min then incubated for 48 h at 37°C. The staining buffer was refreshed after 24 h. The samples were then cleared in 70% ethanol, dissected, and photographed as described above. To ensure an unbiased methodological approach and morphological assessment of *GUS* staining in the leaves, the samples were stained, cleared, and photographed without prior knowledge of the genotype using a double-blind methodology. After decoding the genotypes, staining was compared in three randomly selected leaflets of <4 mm in length from *crd-4* and wild-type plants carrying the *DR5::GUS* reporter in addition to a randomly selected leaflet <8 mm in length from each of the two genotypes.

Accession Numbers

Sequence data from this article can be found in the GenBank/EMBL data libraries under accession numbers shown in Supplementary Table S2.

Supplemental Materials

The following supplemental materials are available.

Supplemental Figure S1. Representative images of leaves or leaflets from F1 plants of crosses between putative mutant lines carrying the *crd* phenotype.

Supplemental Figure S2. The G628A SNP in *crd-2* affects *PsYUC1* splicing.

Supplemental Figure S3. Alignment of Crispoid protein from three wild-type and mutant lines.

Supplemental Figure S4. No portion of *Crispoid/PsYUC1* could be amplified from *crd-3* mutant genomic DNA template.

Supplemental Figure S5. Photosynthetic rate/internal CO_2 concentration curves for WT-4 and *crd-4* mutant plants.

Supplemental Figure S6. Mean dry shoot biomass and plant height in wild-type and *crd* plants.

Supplemental Figure S7. Missing and underdeveloped tendrils in the *crd-1* mutant leaves.

Supplemental Figure S8. Missing and underdeveloped tendrils and pinnae in leaves of the *crd-3* mutant.

Supplemental Figure S9. GUS expression in F2 segregant plants.

Supplemental Figure S10. Mean levels of free IAA from whole aerial potions of 14-d-old seedlings of WT-4 and *crd-4* mutant plants.

Supplemental Table S1. Mean secondary and tertiary vein densities in leaves of allelic *crd* mutants and respective wild-types.

Supplemental Table S2. Accession numbers of proteins used for phylogenetic analysis.

Supplemental Table S3. Details of *Crd* primers used in this study.

ACKNOWLEDGMENTS

The authors thank Charly Potter for preparation of libraries for RNA-seq, Caron James for Sanger sequencing, Vincent Vadez for helpful discussions, Patricia Polowick for generously providing the RTP9 line carrying the *DR5::GUS* insert, Noel Ellis for statistical advice and comments on the manuscript, and two reviewers for astute recommendations on auxin quantifications.

Received June 19, 2017; accepted July 18, 2017; published July 21, 2017.

LITERATURE CITED

Allen GC, Flores-Vergara MA, Krasynanski S, Kumar S, Thompson WF (2006) A modified protocol for rapid DNA isolation from plant tissues using cetyltrimethylammonium bromide. Nat Protoc **1:** 2320–2325

Alves-Carvalho S, Aubert G, Carrère S, Cruaud C, Brochot A-L, Jacquin F, Klein A, Martin C, Boucherot K, Kreplak J, et al (2015) Full-length *de novo* assembly of RNA-seq data in pea (*Pisum sativum* L.) provides a gene expression atlas and gives insights into root nodulation in this species. Plant J **84:** 1–19

Benjamini Y, Hochberg Y (1995) Controlling the false discovery rate: a practical and powerful approach to multiple testing. J R Stat Soc B **57:** 289–300

Bennett T, Hines G, Leyser O (2014) Canalization: what the flux? Trends Genet **30:** 41–48

Berdnikov VA, Gorel' FL, Kosterin OE (2000) A new allele at *Crd* distrubs development of the compound leaf. Pisum Genet **32:** 6–8

Berger D, Altmann T (2000) A subtilisin-like serine protease involved in the regulation of stomatal density and distribution in *Arabidopsis thaliana*. Genes Dev **14:** 1119–1131

Boyce CK, Brodribb TJ, Feild TS, Zwieniecki MA (2009) Angiosperm leaf vein evolution was physiologically and environmentally transformative. Proc Biol Sci **276:** 1771–1776

Brodribb TJ, Feild TS (2000) Stem hydraulic supply is linked to leaf photosynthetic capacity: evidence from New Caledonian and Tasmanian rainforests. Plant Cell Environ **23:** 1381–1388

Brodribb TJ, Feild TS (2010) Leaf hydraulic evolution led a surge in leaf photosynthetic capacity during early angiosperm diversification. Ecol Lett **13:** 175–183

Brodribb TJ, Feild TS, Jordan GJ (2007) Leaf maximum photosynthetic rate and venation are linked by hydraulics. Plant Physiol **144:** 1890–1898

Brodribb TJ, Feild TS, Sack L (2010) Viewing leaf structure and evolution from a hydraulic perspective. Funct Plant Biol **37:** 488–498

Brodribb TJ, Holbrook NM (2005) Water stress deforms tracheids peripheral to the leaf vein of a tropical conifer. Plant Physiol **137:** 1139–1146

Brodribb TJ, Holbrook NM, Zwieniecki MA, Palma B (2005) Leaf hydraulic capacity in ferns, conifers and angiosperms: impacts on photosynthetic maxima. New Phytol **165:** 839–846

Brodribb TJ, Jordan GJ (2011) Water supply and demand remain balanced during leaf acclimation of *Nothofagus cunninghamii* trees. New Phytol **192:** 437–448

Buckley TN, John GP, Scoffoni C, Sack L (2015) How does leaf anatomy influence water transport outside the xylem? Plant Physiol **168:** 1616–1635

Caringella MA, Bongers FJ, Sack L (2015) Leaf hydraulic conductance varies with vein anatomy across *Arabidopsis thaliana* wild-type and leaf vein mutants. Plant Cell Environ **38:** 2735–2746

Carins Murphy MR, Jordan GJ, Brodribb TJ (2012) Differential leaf expansion can enable hydraulic acclimation to sun and shade. Plant Cell Environ **35:** 1407–1418

Carins Murphy MR, Jordan GJ, Brodribb TJ (2016) Cell expansion not cell differentiation predominantly co-ordinates veins and stomata within and among herbs and woody angiosperms grown under sun and shade. Ann Bot (Lond) **118:** 1127–1138

Cheng Y, Dai X, Zhao Y (2006) Auxin biosynthesis by the YUCCA flavin monooxygenases controls the formation of floral organs and vascular tissues in *Arabidopsis*. Genes Dev **20:** 1790–1799

Cheng Y, Dai X, Zhao Y (2007) Auxin synthesized by the YUCCA flavin monooxygenases is essential for embryogenesis and leaf formation in *Arabidopsis.* Plant Cell **19:** 2430–2439

Cook SD, Nichols DS, Smith J, Chourey PS, McAdam EL, Quittenden L, Ross JJ (2016) Auxin biosynthesis: are the indole-3-acetic acid and phenylacetic acid biosynthesis pathways mirror images? Plant Physiol **171:** 1230–1241

Dalmais M, Schmidt J, Le Signor C, Moussy F, Burstin J, Savois V, Aubert G, Brunaud V, de Oliveira Y, Guichard C, et al (2008) UTILLdb, a *Pisum sativum in silico* forward and reverse genetics tool. Genome Biol **9:** R43–R43

Demason DA, Chetty V, Barkawi LS, Liu X, Cohen JD (2013) *Unifoliata-Afila* interactions in pea leaf morphogenesis. Am J Bot **100:** 478–495

DeMason Darleen A, Polowick Patricia L (2009) Patterns of DR5:GUS expression in organs of pea (*Pisum sativum*). Int J Plant Sci **170:** 1–11

Domoney C, Knox M, Moreau C, Ambrose M, Palmer S, Smith P, Christodoulou V, Isaac PG, Hegarty M, Blackmore T, et al (2013) Exploiting a fast neutron mutant genetic resource in *Pisum sativum* (pea) for functional genomics. Funct Plant Biol **40:** 1261–1270

Feugier FG, Mochizuki A, Iwasa Y (2005) Self-organization of the vascular system in plant leaves: inter-dependent dynamics of auxin flux and carrier proteins. J Theor Biol **236:** 366–375

Fiorin L, Brodribb TJ, Anfodillo T (2016) Transport efficiency through uniformity: organization of veins and stomata in angiosperm leaves. New Phytol **209:** 216–227

Kanaoka MM, Pillitteri LJ, Fujii H, Yoshida Y, Bogenschutz NL, Takabayashi J, Zhu J-K, Torii KU (2008) SCREAM/ICE1 and SCREAM2 specify three cell-state transitional steps leading to *arabidopsis* stomatal differentiation. Plant Cell **20:** 1775–1785

Laucou V, Haurogné K, Ellis N, Rameau C (1998) Genetic mapping in pea. 1. RAPD-based genetic linkage map of *Pisum satium.* Theor Appl Genet **97:** 905–915

Le J, Liu X-G, Yang K-Z, Chen X-L, Zou J-J, Wang H-Z, Wang M, Vanneste S, Morita M, Tasaka M, et al (2014) Auxin transport and activity regulate stomatal patterning and development. Nat Commun **5:** 3090

Le SQ, Gascuel O (2008) An improved general amino acid replacement matrix. Mol Biol Evol **25:** 1307–1320

Lee S-W, Feugier FG, Morishita Y (2014) Canalization-based vein formation in a growing leaf. J Theor Biol **353:** 104–120

Liu H, Ying Y-Y, Zhang L, Gao Q-H, Li J, Zhang Z, Fang J-G, Duan K (2012) Isolation and characterization of two YUCCA flavin monooxygenase genes from cultivated strawberry (*Fragaria* × *ananassa* Duch.). Plant Cell Rep **31:** 1425–1435

Mashiguchi K, Tanaka K, Sakai T, Sugawara S, Kawaide H, Natsume M, Hanada A, Yaeno T, Shirasu K, Yao H, et al (2011) The main auxin biosynthesis pathway in *Arabidopsis.* Proc Natl Acad Sci USA **108:** 18512–18517

Mattsson J, Ckurshumova W, Berleth T (2003) Auxin signaling in *Arabidopsis* leaf vascular development. Plant Physiol **131:** 1327–1339

Mattsson J, Sung ZR, Berleth T (1999) Responses of plant vascular systems to auxin transport inhibition. Development **126:** 2979–2991

McAdam SAM, Brodribb TJ, Ross JJ (2016) Shoot-derived abscisic acid promotes root growth. Plant Cell Environ **39:** 652–659

Mitchison GJ (1980) Model for vein formation in higher-plants. Proc R Soc Lond B Biol Sci **207:** 79–109

Mortazavi A, Williams BA, McCue K, Schaeffer L, Wold B (2008) Mapping and quantifying mammalian transcriptomes by RNA-Seq. Nat Methods **5:** 621–628

Novák O, Hényková E, Sairanen I, Kowalczyk M, Pospíšil T, Ljung K (2012) Tissue-specific profiling of the *Arabidopsis thaliana* auxin metabolome. Plant J **72:** 523–536

Paradis E, Claude J, Strimmer K (2004) APE: analyses of phylogenetics and evolution in R language. Bioinformatics **20:** 289–290

Rolland-Lagan AG, Prusinkiewicz P (2005) Reviewing models of auxin canalization in the context of leaf vein pattern formation in *Arabidopsis.* Plant J **44:** 854–865

Sachs T (1981) The control of the patterned differentiation of vascular tissue. Adv Bot Res **9:** 151–262

Sack L, Cowan PD, Jaikumar N, Holbrook NM (2003) The 'hydrology' of leaves: co-ordination of structure and function in temperate woody species. Plant Cell Environ **26:** 1343–1356

Sack L, Frole K (2006) Leaf structural diversity is related to hydraulic capacity in tropical rain forest trees. Ecology **87:** 483–491

Sack L, Scoffoni C (2013) Leaf venation: structure, function, development, evolution, ecology and applications in the past, present and future. New Phytol **198:** 983–1000

Sack L, Scoffoni C, John GP, Poorter H, Mason CM, Mendez-Alonzo R, Donovan LA (2013) How do leaf veins influence the worldwide leaf economic spectrum? Review and synthesis. J Exp Bot **64:** 4053–4080

Scarpella E, Meijer AH (2004) Pattern formation in the vascular system of monocot and dicot plant species. New Phytol **164:** 209–242

Schliep KP (2011) phangorn: phylogenetic analysis in R. Bioinformatics **27:** 592–593

Scoffoni C, Chatelet DS, Pasquet-Kok J, Rawls M, Donoghue MJ, Edwards EJ, Sack L (2016) Hydraulic basis for the evolution of photosynthetic productivity. Nat Plants **2:** 16072

Scoffoni C, Kunkle J, Pasquet-Kok J, Vuong C, Patel AJ, Montgomery RA, Givnish TJ, Sack L (2015) Light-induced plasticity in leaf hydraulics, venation, anatomy, and gas exchange in ecologically diverse Hawaiian lobeliads. New Phytol **207:** 43–58

Scoffoni C, Rawls M, McKown A, Cochard H, Sack L (2011) Decline of leaf hydraulic conductance with dehydration: relationship to leaf size and venation architecture. Plant Physiol **156:** 832–843

Sievers F, Wilm A, Dineen D, Gibson TJ, Karplus K, Li W, Lopez R, McWilliam H, Remmert M, Söding J, et al (2011) Fast, scalable generation of high-quality protein multiple sequence alignments using Clustal Omega. Mol Sys Biol **7:** 539

Swiecicki WK (1989) A new gene *CRISPOID* (*crd*) on chromosome 1. Pisum Newsletter **21:** 73–74

Tao Y, Ferrer J-L, Ljung K, Pojer F, Hong F, Long JA, Li L, Moreno JE, Bowman ME, Ivans LJ, et al (2008) Rapid synthesis of auxin via a new tryptophan-dependent pathway is required for shade avoidance in plants. Cell **133:** 164–176

Tayeh N, Aluome C, Falque M, Jacquin F, Klein A, Chauveau A, Bérard A, Houtin H, Rond C, Kreplak J, et al (2015) Development of two major resources for pea genomics: the GenoPea 13.2K SNP Array and a high-density, high-resolution consensus genetic map. Plant J **84:** 1257–1273

Tivendale ND, Davies NW, Molesworth PP, Davidson SE, Smith JA, Lowe EK, Reid JB, Ross JJ (2010) Reassessing the role of *N*-hydroxytryptamine in auxin biosynthesis. Plant Physiol **154:** 1957–1965

Tobeña-Santamaria R, Bliek M, Ljung K, Sandberg G, Mol JNM, Souer E, Koes R (2002) FLOOZY of petunia is a flavin mono-oxygenase-like protein required for the specification of leaf and flower architecture. Genes Dev **16:** 753–763

Tyree MT, Zimmermann MH (2002) Xylem structure and the ascent of sap. Springer, Berlin

Verna C, Sawchuk MG, Linh NM, Scarpella E (2015) Control of vein network topology by auxin transport. BMC Biol **13:** 94

Wong SC, Cowan IR, Farquhar GD (1979) Stomatal conductance correlates with photosynthetic capacity. Nature **282:** 424–426

Yu G, Smith DK, Zhu H, Guan Y, Lam TT-Y (2017) ggtree: an R package for visualization and annotation of phylogenetic trees with their covariates and other associated data. Methods Ecol Evol **8:** 28–36

Zhang S-B, Sun M, Cao K-F, Hu H, Zhang J-L (2014) Leaf photosynthetic rate of tropical ferns is evolutionarily linked to water transport capacity. PLoS One **9:** e84682

Zhao Y (2012) Auxin biosynthesis: a simple two-step pathway converts tryptophan to indole-3-acetic acid in plants. Mol Plant **5:** 334–338

Zhao Y, Christensen SK, Fankhauser C, Cashman JR, Cohen JD, Weigel D, Chory J (2001) A role for flavin monooxygenase-like enzymes in auxin biosynthesis. Science **291:** 306–309

Zsögön A, Negrini AC, Peres LEP, Nguyen HT, Ball MC (2015) A mutation that eliminates bundle sheath extensions reduces leaf hydraulic conductance, stomatal conductance and assimilation rates in tomato (*Solanum lycopersicum*). New Phytol **205:** 618–626